HHS Public Access

Author manuscript

Magn Reson Med. Author manuscript; available in PMC 2019 March 01.

Published in final edited form as:

Magn Reson Med. 2018 March ; 79(3): 1304–1313. doi:10.1002/mrm.26763.

Three-dimensional mapping of brain venous oxygenation using R_2^* oximetry

Deng Mao[1,2], **Yang Li**[1,2], **Peiying Liu**[1], **Shin-Lei Peng**[1,3], **Jay J. Pillai**[1], and **Hanzhang Lu**[1]

[1]The Russell H. Morgan Department of Radiology & Radiological Science, Johns Hopkins University School of Medicine, Baltimore, MD, USA

[2]Graduate School of Biomedical Sciences, University of Texas Southwestern Medical Center, Dallas, Texas, USA

[3]Department of Biomedical Imaging and Radiological Science, China Medical University, Taichung, Taiwan

Abstract

Purpose—Cerebral venous oxygenation (Y_v) is an important biomarker for brain diseases. This study aims to develop an R_2^*-based MR oximetry that can measure cerebral Y_v in 3D.

Methods—This technique separates blood signal from tissue by velocity-encoding phase contrast and measures the R_2^* of pure blood by multi-gradient-echo acquisition. The blood R_2^* was converted to Y_v using an R_2^*-vs-oxygenation (Y) calibration curve, which was obtained by in vitro bovine blood experiments. Reproducibility, sensitivity, validity, and resolution dependence of the technique were evaluated.

Results—In vitro R_2^*-Y calibration plot revealed a strong dependence of blood R_2* on oxygenation, with additional dependence on hematocrit. In vivo results demonstrated that the technique can provide a 3D venous oxygenation map that depicts both large sinuses and smaller cortical veins, with venous oxygenation ranging from 57% to 72%. Intra-session coefficient-of-variation of the measurement was 3.0%. The technique detected an average Y_v increase of 10.8% due to hyperoxia, which was validated by global oxygenation measurement from TRUST. Two spatial resolutions, one with an isotropic voxel dimension and the other with a non-isotropic dimension, were tested for full brain coverage.

Conclusion—This study demonstrated the feasibility of 3D brain oxygenation mapping without using contrast agent.

Keywords

MR oximetry; blood R_2^*; blood oxygenation; hyperoxia; phase contrast; venogram

Corresponding author: Hanzhang Lu, Ph.D., The Russell H. Morgan Department of Radiology & Radiological Science, Johns Hopkins University School of Medicine, 600 N. Wolfe Street, Park 322, Baltimore, MD 21287, hanzhang.lu@jhu.edu, Phone: 410-955-1431, Fax: 410-614-1977.

Introduction

Cerebral venous oxygenation (Y_v) is closely associated with the brain's oxygen extraction, metabolism, and to some extent neural activity, and is a promising biomarker in several major neurological diseases including stroke (1,2), tumor (3) and Alzheimer's disease (4-6). However, measurement of cerebral venous oxygenation in humans has proven difficult. ^{15}O positron emission tomography (PET) was one of the first methods developed to measure Y_v, but this method requires inhalation of radioactive gas, arterial blood sampling, and an onsite cyclotron to produce the short half-life ^{15}O tracer (7). As a result, only a small number of laboratories are still performing such experiments in recent years.

An active research topic in the MRI field is, therefore, the development of new techniques to non-invasively measure Y_v in humans. To this end, measurement of global, whole-brain venous oxygenation is now relatively well-established. One can either use the T_2-Relaxation-Under-Spin-Tagging (TRUST) (8) or phase susceptometry method (9) to determine cerebral Y_v within approximately one minute. In contrast, considerable technical development is still needed for MRI techniques of regional Y_v quantification, which would have a greater potential for clinical applications. While all such techniques are based on the paramagnetic property of deoxyhemoglobin, different types of methods have focused on magnitude (10-12) or phase (13,14) manifestations of these effects. One particular line of techniques is based on a calibratable relationship between blood R_2 (or R_2^*) and oxygenation (Y) (15-17). By designing advanced MR pulse sequences to accurately measure blood transverse relaxation in vivo, one can obtain a quantitative assessment of cerebral oxygenation without using any contrast agent or physiological challenge. Although several efforts have demonstrated promising results (18-20), the spatial coverage of these prior works has been limited to a single slice. Therefore, in order to have a practical utility in clinical settings, expansion of these techniques to 3D, ideally with whole-brain coverage, is highly desirable.

The goal of this study is to develop 3D acquisition and analysis schemes to measure blood oxygenation in human cerebral veins after accounting for partial voluming between blood and tissue. The proposed method employs velocity-encoded phase contrast imaging to differentiate flowing blood signal from static tissue, and applies flow-compensated multi-gradient-echo acquisition to rapidly map blood R_2^*. In vivo experiments were performed to demonstrate the feasibility and reproducibility of this method. Sensitivity of the method to known effect of oxygenation change was tested by hyperoxia physiological challenge. In vitro experiments were performed to establish the R_2^*-Y calibration plot, from which the in vivo R_2^* values could be converted to physiological value of venous oxygen saturation fraction. Validation was performed by comparing the Y_v measured with this new sequence to an established method of global Y_v (21). Finally, tradeoff between in-plane and through-plane resolution in 3D acquisition was investigated.

Methods

Pulse sequence

As shown in Figure 1, the proposed sequence is a multi-gradient echo phase contrast sequence. Using the phase contrast principle, a complex difference (CD) image can be obtained by the complex subtraction of two images acquired with opposite gradient polarity (green gradients in Figure 1). Only the flowing blood signal is present in the CD image, thereby isolating pure blood signal in the presence of tissue partial voluming. The multi-gradient echo acquisition then allows the measurement of blood R_2^* (or T_2^*). Flow compensation was employed in both y and z directions for the first echo. Additional flow compensation in the y-direction was applied for all later echoes using schemes developed by Xu et al. (14). These strategies are important in minimizing mis-match in spatial coordinates of the measured signal, so-called oblique flow artifacts (22). Fly-back gradients are applied in the readout direction to ensure identical geometric distortion along x-direction across all echoes (23). Compared to a previous sequence which was based on a similar principle but used CPMG-T_2 preparation pulses (19), the present sequence is more time efficient in three ways. First, the multiple echoes are acquired in one TR, rather than in separate TRs. Second, the CPMG-T_2 sequence is associated with higher RF power deposition, thus a relatively long TR (e.g. 668 ms) is needed to accommodate the SAR limits. Third, since T_2^* is considerably shorter than CPMG-T_2, a shorter echo time can be used for the same amount of signal attenuation, which reduces TR. These improvements add up to approximately 40 times reduction in scan time compared to the previous method (19), and allow the extension of the technique from 2D to 3D without drastically increasing the scan duration. To be consistent with the naming convention of the previous method (19), we referred to the present sequence as T_2-Relaxation-Under-Phase-Contrast 3D version (TRU-PC 3D).

Theory

The blood signal as measured in the CD image is related to flow velocity and cutoff velocity of the sequence, V_{enc}, by:

$$\mathrm{CD}=2M_{\mathrm{blood}}\left|\sin\left(\frac{\pi\nu}{2V_{\mathrm{enc}}}\right)\right| \quad [1]$$

where M_{blood} is the magnetization of the blood at given TE and v is the velocity of the blood along the encoding direction (typically anterior-posterior, foot-head, or left-right). M_{blood} is related to TE, TR, and flip angle of the sequence as well as its volume fraction in the voxel, and can be written as:

$$M_{\mathrm{blood}}(TE)=M_0\cdot f_{\mathrm{blood}}\cdot\frac{\sin\alpha\cdot(1-e^{-TR\cdot R_{1,\mathrm{blood}}})}{1-\cos\alpha\cdot e^{-TR\cdot R_{1,\mathrm{blood}}}}\cdot e^{-TR\cdot R^*_{2,\mathrm{blood}}} \quad [2]$$

where M_0 is the total equilibrium magnetization in the voxel, f_{blood} is the fraction of blood, and α is the flip angle. When we combine Eqs. [1] and [2], the CD signal at the given TE can be written as:

$$CD(TE)=2M_0 \cdot f_{\text{blood}} \cdot \left|\sin\left(\frac{\pi\nu}{2V_{\text{enc}}}\right)\right| \cdot \frac{\sin\alpha \cdot (1-e^{-TR\cdot R_{1,\text{blood}}})}{1-\cos\alpha \cdot e^{-TR\cdot R_{1,\text{blood}}}} \cdot e^{-TR\cdot R^*_{2,\text{blood}}} \quad [3]$$

In this equation, if we combine the TE-independent terms into a S_0, the signal becomes:

$$CD(TE)=S_0 e^{-TE\cdot R^*_{2,\text{blood}}} \quad [4]$$

The $R^*_{2,\text{blood}}$ can then be estimated from a mono-exponential fitting of the multi-TE data.

In vivo experiment

The MRI experiment was carried out in a total of 13 young and healthy subjects (age, 27±7 years; range, 21-35, 3 males) using a 3 Tesla MRI scanner (Philips Healthcare, Best, The Netherlands). The protocol was approved by local Institutional Review Board. All subjects gave informed written consent before participating in the study. The RF transmission used the body coil, and the receiving coil was a 32-channel head coil. Three sub-studies were conducted to characterize different aspects of the technique, which are described separately in the following sections.

Feasibility and reproducibility study

Four subjects participated in this sub-study. Each participant underwent two TRU-PC 3D scans and a time-of-flight (TOF) angiogram scan, which was used in data analysis (see below) to differentiate veins from arteries in the TRU-PC 3D al orientation, anterior-posterior phase encoding, FOV=200×200×85image. The imaging parameters for TRU-PC 3D were as follows: 3D gradient echo readout, sagitt mm^3, acquisition matrix=288×284×17, voxel size=0.7×0.7×5 mm^3, bandwidth=217 Hz, V_{enc}=9 cm/s in anterior-posterior direction, flip angle/TE/ΔTE/TR= 15.6°/13 ms/14 ms/60 ms, 4 echoes were acquired for each TR. In choosing echo time parameters, our goal was to use the shortest possible TE and ΔTE for given gradient amplitude and slew rate while maintaining flow compensation. The number of echoes was determined based on considerations of sufficient signal decay while minimizing TR (thereby scan duration). The scan time of each TRU-PC 3D was 9.8 min. The imaging parameters for TOF MRI were as follows: 3D gradient echo readout, axial slice orientation divided into 10 chunks, FOV=170×170×150 mm^3, acquisition matrix=356×226×300, voxel size=0.48×0.75×1 mm^3, flip angle/TE/TR=20°/3.5 ms/25 ms, Sensitivity encoding (SENSE) factor=2, scan duration=10.2 min. Note that the FOVs of the TRU-PC 3D and TOF scans are not matched because they are acquired in different orientations. In post-processing, however, these images are resliced to match each other.

Hyperoxia study

A hyperoxia study was performed to test the sensitivity of TRU-PC 3D to expected venous oxygenation change when the subject inhales high oxygen content gas. Four subjects participated in this sub-study. During the experiment, the subjects were instructed to inhale room air and high oxygen content gas sequentially (95% O_2) through mouth piece as described previously (24). The gas type the subject inhaled was controlled though a three way valve. During the room air period, a TRU-PC 3D and global oxygenation sequence, TRUST MRI (8), were performed. The TRU-PC 3D protocol was identical to that used in the feasibility study described above. The TRUST sequence was described in previous literature (8) and had a duration of 1.2 minutes. A TOF angiogram scan was then started. Half way (approximately 5 minutes) into the TOF scan, the gas valve was switched to allow the participant to start breathing the hyperoxic gas. By the time the TOF scan is completed, the participant would have breathed the hyperoxic gas for about 5 minutes and is expected to have reached a new steady state. Then TRU-PC 3D and TRUST MRI were performed again under the hyperoxic state.

Resolution-dependence study

We studied the tradeoff between in-plane and through-plane resolution in a full-brain coverage scan. Two TRU-PC 3D protocols were compared in 5 subjects. The first protocol used a high in-plane resolution and a low through-plane resolution with a voxel size of 0.7×0.7×5 mm^3, a matrix of 288×284×31, and a scan duration of 17.9 min. The other protocol used a more isotropic voxel size of 1.5×1.5×2 mm^3, acquisition matrix of 133×132×77, and a scan time of 20.6 min. A TOF angiogram was also performed.

In vivo data analysis

The TRU-PC 3D images were reconstructed and corrected for eddy-current induced phase artifact as described in (25). To focus our analysis on voxels containing measurable blood vessels, the complex difference images from all TEs were averaged and a threshold (10 times the standard deviation of the noise sampled from a non-vessel control region) was applied to obtain a preliminary vessel mask. Further analysis of blood oxygenation was only conducted on voxels within the mask.

Blood oxygenation was quantified on two spatial levels, region-of-interest (ROI) level and voxel-wise level. In the ROI analysis, nine ROIs were drawn on the vessel mask to encompass five mid-sagittal and four cortical veins: anterior and posterior superior sagittal sinus, internal cerebral veins, straight sinus, left transverse sinus, bilateral anterior and posterior cortical veins. The complex difference signal inside the ROI was averaged for each TE and fitted monoexponentially for R_2^*. The R_2^* was further converted to oxygenation according the R_2^*-Y calibration plot, which is discussed in the next section.

For voxel-wise analysis, an isotropic Gaussian smoothing (6mm full-width-half-maximum, FWHM) was applied to the masked complex difference images. Voxel-wise R_2^* fitting was performed to voxels within the vessel mask. To avoid arterial vessels and to remove voxels with low signal stability, the following four steps were performed to refine the mask used for final display. First, an artery mask was obtained by analyzing the time-of-flight angiogram

using the Amira software (FEI Visualization Sciences Group, Hillsboro, Oregon) and voxels in the arterial mask were eliminated from the blood R_2^* map. Second, 95% confidence interval of the R_2^* estimation was evaluated and voxels that have a confidence interval of greater than the estimated R_2^* value were discarded. Third, the S_0 value from the R_2^* fitting, which denotes the intensity of blood signal without any R_2^* weighting, was evaluated and voxels with an S_0 of less than a threshold (1×10^5 A.U. for voxel size $0.7\times0.7\times5$ mm^3 and 3×10^5 A.U. for voxel size $1.5\times1.5\times2$ mm^3) were discarded. Note that we used a group-level threshold for S_0. An alternative approach would be to use an individual threshold based on each data's SNR. We did not use an SNR-based threshold because the estimation of noise in S_0 is not trivial as it is a fitted parameter rather than experimental measure. Finally, small clusters with a volume of less than 135 mm^3 were removed. The final R_2^* map was converted to oxygenation map using the calibration plot. For 3D display purposes, we employed the Amira software to convert the oxygenation map to a 3D model. The oxygenation value was then displayed on Paraview (26) in vtk format.

In vitro blood experiment and analysis

To allow the conversion of blood R_2^* value to oxygen saturation fraction, we conducted a set of calibration experiments using bovine blood, which has physiological and MR properties comparable to human blood (27). Note that the calibration experiment does not need to be done for every subject or every study. Once a calibration plot is established, it can be used for all future scans using an equivalent pulse sequence. Fresh Bovine blood was obtained from a local slaughtering house in the morning of each experimental day. Sodium citrate was added to the blood for 25 mM concentration to avoid coagulation. The experiments were completed within 8 h after collection to minimize the effect of degradation. Adjustment of hematocrit (Hct) level was achieved by centrifuging the blood and adding or removing plasma. Four Hct levels (36%, 39%, 45% and 53%) were studied in 3 batches of blood. Adjustment of blood oxygenation was achieved by exposure to room air (to increase oxygenation) or nitrogen gas (to decrease oxygenation). For blood MR measurements, 10 ml of blood was placed in a 27 mm-diameter plastic tube and kept at 37 °C with water bath to match the physiological condition. The blood oxygenation and hematocrit levels were measured by a blood gas analyzer (ABL830m, Radiometer America Inc., Westlake, OH) immediately before and after the MR session and their averaged value was used in the analysis. The imaging protocol was the same as the in vivo protocol used in the reproducibility study, except that the FOV was reduced to 90×90 mm^2 to shorten the scan time to 4.4 min. The MR session for one oxygenation and Hct level was completed within 6 min. According to our previous experience (15,28), blood cell precipitation is minimal within this short time.

For data analysis, ROIs were drawn in the center of three consecutive slices encompassing the blood sample. The signals in the ROIs were averaged and fitted to a mono-exponential equation:

$$S=S_0e^{-TE\cdot R_2^*}$$

The resulting R_2^* values were then fitted to a quadratic function of blood oxygenation, Y (16,29):

$$R_2^* = A^* + C^*(1 - Y)^2$$

This fitting was performed for each Hct level. Linear interpolation of the R_2^*-Y curves across Hct then yields a 3D calibration plane for all physiological Hct levels.

The calibration plot was used to convert in vivo R_2^* values to oxygenation. In this study, we assumed an Hct of 0.42 for male and 0.40 for female. Because human scans tend to have more macroscopic inhomogeneities due to imperfect shimming, this will increase R_2^*. Thus, a fixed correction factor $R_{2,\mathrm{corr}}^*$ was subtracted from in vivo R_2^* before the conversion. In this study, $R_{2,\mathrm{corr}}^*$ was assumed to be 8.8 s^{-1} based on the literature (30). Note that since a fixed $R_{2,\mathrm{corr}}^*$ is used, this assumption will not change any inter-subject or inter-regional differences of the oxygenation results.

Results

Blood R_2^* and its dependence on oxygenation and Hct

The fitting of in vitro blood signal as a function of TE was reliable, and R_2^* could be estimated from all blood samples. Figure 2a shows the dependence of blood R_2^* on oxygenation for a range of Hct values. As expected, blood R_2^* is strongly dependent on Y. For a typical Hct level of 39%, R_2^* of a venous blood sample with oxygenation of 60% was 28.9 s^{-1}, while R_2^* of a fully oxygenated blood sample was 12.7 s^{-1}. In contrast, blood R_2^* is less affected by Hct. Fitting the R_2^* value to a quadratic equation of Y yielded coefficients A and C, which are listed in Table 1 for each Hct value. The Hct-specific 2D curves were extended to a 3D surface plot, by interpolating the curves along the Hct dimension, so that one can obtain an R_2^*-Y plot for any Hct value within the physiological range (Figure 2b).

Feasibility study of TRU-PC 3D

An example of complex difference images from a TRU-PC 3D scan are shown in Figure 3a. Multiple slices along the left-right direction have been combined (via maximum intensity projection) for display purposes. Large venous vessels such as internal cerebral veins (arrows) and superior sagittal sinus (arrows heads) are discernible in the images. Furthermore, small cortical and sub-cortical vessels that do not have designated names are also visible, which is an advantage of the 3D method in comparison with previous single-slice technique. As echo time increases (Figure 3b), the signal intensity decreases, the rate of which is blood R_2^*.

ROI results of 9 different venous structures (Figure 4), of which five were major veins and four were cortical veins, are listed in Table 2. The venous oxygenation ranged from 57% to 72%, which is in agreement with reported Y_v values in the literature (31-33). Results of

intra-session test-retest reproducibility are also shown in Table 2. The average coefficient-of-variation (CoV) across runs is 3.0%.

3D oxygenation maps of veins and arteries (separated based on TOF angiogram) as well as their combination are displayed in Figure 5a. It can be seen that, in the venous oxygenation map, most of the voxels have blue color, consistent with the expected lower oxygenation range. In contrast, the arterial oxygenation map largely shows red color, indicative of higher oxygenation values. Histograms of all voxels of all subjects (N=13, 3M, Age 26.5±3.6 years old) are displayed in Figure 5b, providing a quantitative summary of the oxygenation values in the voxels.

Hyperoxia study

Hyperoxia increased the subjects' end-tidal O_2 from 13.3%±0.3% to 85.0%±2.9%, while end-tidal CO_2 did not show a change (5.8%±0.1% and 5.6%±0.3% during room-air and hyperoxia, respectively). Venous oxygenation maps during room-air and hyperoxia are shown in Figure 6a. It can be seen that blood oxygenation clearly becomes higher during hyperoxia, consistent with the known effects of this physiological manipulation. ROI results are shown in Figure 6b, which revealed that venous oxygenation increased significantly (P<0.05) in every region and by 10.8% on average.

Venous oxygenation values measured by TRU-PC 3D were compared with those measured by a well-established global method, TRUST MRI. For this analysis, data from 8 subjects were used, including 4 participants from the hyperoxia study (who provided 4 hyperoxia data points and 4 room-air data points) and 4 participants from the feasibility study (who provided 4 room-air data points). The average oxygenation from TRU-PC 3D was 65.0% ±7.4%, which was similar (P=0.8) to the TRUST results of 64.8%±7.7%. Figure 7 showed a scatter plot of individual participants, revealing a strong correlation (P<0.001) between the two methods.

Resolution-dependence study

Figure 8 shows venous oxygenation maps acquired at two spatial resolutions (see Supporting Video S1). Panel (a) was acquired with a high in-place resolution (0.5×0.5 mm^2), but a coarse through-plane resolution (5 mm). Panel (b) was acquired with a more isotropic voxel dimensions of 1.5×1.5×2 mm^3. It can be seen that each scheme has advantages and disadvantages. The scan with high in-plane resolution shows good spatial acuity when viewed sagittally, but appears poorly in the coronal view. A movie for the two maps is provided in the supporting information for better view (Supporting Video S1). The isotropic scan shows a more consistent image when viewed from different directions. ROI analysis showed no difference (P>0.05 for all ROIs) in oxygenation between the two methods, with 56.0%±9.0% (N=5) for the non-isotropic protocol and 57.9%±9.3% for the isotropic protocol.

Discussion

This study presented a technique for quantitative assessment of brain venous oxygenation without using exogenous contrast agent. The technique is based on a novel pulse sequence

and, compared to previous methods, has extended spatial coverage. The performance of this new method was demonstrated in a group of healthy volunteers and the results showed oxygenation values within the typical physiological range. The method was found to be reproducible with intra-session CoV of 3% and was sensitive to oxygenation changes induced by hyperoxia. The method showed good agreement with a validated technique TRUST MRI. In vitro experiments were also performed to characterize the relationship between blood R_2^* and oxygenation, which was used to convert in vivo R_2^* results to oxygen saturation fractions.

Physiological considerations

The brain represents approximately 2% of the body weight, but consumes about 20% of the energy (34). Thus, the rate of oxygen metabolism is an important marker for brain development, aging, and diseases. Venous oxygenation is closely related to cerebral metabolic rate of oxygen ($CMRO_2$) and oxygen extraction fraction (OEF),

$\mathrm{OEF}=\frac{(Y_\alpha - Y_\nu)}{Y_\alpha}$ and $CMRO_2 = \mathrm{CBF} \cdot (Y_a - Y_v)$. Among these physiological parameters, arterial oxygenation (Y_a) is relatively easy to measure and cerebral blood flow (CBF) can also be evaluated with a number of non-invasive techniques. Assessment of Y_v has been a bottle neck in terms of measurement technologies. ^{15}O PET is the current gold standard, but it is rarely used due to complexity in procedures. Therefore, at present, there is not an established method to measure brain venous oxygenation in routine clinical practice.

Recently, there has been a growing interest to develop new MR methods to measure Y_v. Indeed, global Y_v measurements using MRI have been successfully applied to Alzheimer's disease (6), multiple sclerosis (35), genetic disease of brain metabolism (36), sickle cell (37), anorexia (38), end-stage renal disease (39), congenital heart disease (40) and cocaine addiction (41). In addition, it has been used in studies of brain development and aging (31). However, application of such techniques in focal brain diseases such as brain tumor and stroke requires regional Y_v methods. The present work represents one of such efforts.

Technical considerations

MRI techniques for regional Y_v quantification can be divided into 4 categories. The first one is a qBOLD method based on biophysical modeling of blood oxygenation on tissue transverse relaxation rate (10). The second one is based on calibrated fMRI. In this method, two gas challenges, for example hyperoxia and hypercapnia, are applied to induce alteration in CBF and BOLD MRI signal. By using a mathematical model to solve the interplay among these physiological parameters, CBF, OEF, and $CMRO_2$ can be simultaneously estimated (11,12). The third category is based on the effect of paramagnetic deoxyhemoglobin on MR signal phase (9,13,14). The method proposed in the present work represents a fourth category, which is based on the relationship between oxygenation and R_2/R_2^* of the blood. The methods in this category involve advanced pulse sequences that are capable of isolating venous blood signal from surrounding tissue, thereby minimizing partial voluming effects. Several techniques have been proposed including those based on spin labeling principles such as TRUST (8), QUIXOTIC (18) and VSEAN (20), and those based on flow-encoded

phase contrast such as TRU-PC (19). However, to date, such methods are spatially limited to a single slice acquisition.

The present work represents the first demonstration of 3D venous oxygenation using blood transverse relaxation measurements. Compared to the 2D TRU-PC method reported by Krishnamurthy et al. (19), the present 3D technique uses a R_2^* approach rather than R_2. This change was made primarily based on scan time considerations. The previous 2D method required approximately 7 minutes to acquire one slice, thus it was not feasible to extend it to 3D acquisitions. One of the reasons for the long scan time of 2D TRU-PC was that the 180° pulses in the R_2 preparation module of the sequence result in considerable RF power deposition and, consequently, a long TR (>668 ms) must be used to be compatible with SAR limits. The 3D sequence proposed in this study does not use refocusing RF pulses, and thus a short TR of 60 ms can be used, which can shorten the scan duration by 11 times with this factor alone. A second factor that reduced scan duration in the TRU-PC 3D technique was that multiple echoes were acquired in the same TR, unlike the 2D method in which different TRs must be used for different T_2-preparation durations. This factor could shorten the scan time by another 4 folds. The scheme of acquiring all echoes in one TR also minimized the effects of subject motion or physiological fluctuations. Collectively, these improvements allowed the assessment of 3D venous oxygenation with only a modest increase in scan time.

The present study used a V_{enc} of 9 cm/s for flow encoding of cerebral veins. This value is approximately the mid-point of the large vessel (15 cm/s) and small vessel (4 cm/s) V_{enc} values used in our previous study (25). Previous literature has suggested the following velocity range for various venous vessels in the brain: superior sagittal sinus 15.2 cm/s (42), straight sinus 10.4 cm/s (43), the great vein 9.8 cm/s (43), internal cerebral veins 6.1 cm/s (43), and cortical vein 7.1 cm/s (44). Thus, the V_{enc} we chose provides a good balance of sensitivity between large and small veins. If more scan time is available, it is recommended to utilize more than one V_{enc} value so that a better sensitivity could be obtained for a range of vessels.

The method proposed in the present work employed flow encoding in the anterior-posterior direction, but can be expanded to the three-directional space. Such expansion could adopt schemes used previously in 3D phase-contrast MRI (45) such as Hadamard encoding. In this encoding scheme, four types of flow-encoding gradients will be used in the experiment and various combinations of these four complex images will yield flow-encoded signal in each of the x, y, and z directions. The three flow-encoded signals can then be combined geometrically to yield the final signal intensity for R_2^* fitting.

The present work has primarily focused on the measurement of oxygenation in cerebral veins. It is also possible to measure oxygenation in arteries (e.g. Figure 5). However, it should be pointed out that, due to the quadratic nature of the blood relaxometry curve (e.g. Figure 2), the sensitivity of our technique is expected to be lower in arterial oxygenation range. Additionally, since arterial blood is originated from the heart and its oxygenation is the same across the body, this value can be measured more conveniently in the periphery using pulse oximetry.

Limitations

While the switch from R_2 to R_2^* measurement increased acquisition efficiency and reduced scan time, it also increased the susceptibility of the sequence to several other factors. In our oxygenation map, we observed some high oxygenation values in the venous map and some low oxygenation values in the arterial map (Figure 5). One possible reason is that, at the time of the flow-encoding (i.e. time of the bipolar gradient), the blood spins that are later measured in the different echoes are physically in different locations. That is, different echoes measured different spins. These spins may have slightly different flow velocity, thus may bias the R_2^* estimation. Another possible reason for the low oxygenation values in the arterial voxels at the base of the brain could be that the blood signals being measured in the later echoes did not experience the excitation RF pulse.

Another limitation is that R_2^* is more sensitive to shimming condition and macroscopic inhomogeneity, compared to R_2. Because in vitro blood samples are more homogeneous and easier to shim relative to in vivo imaging, this results in some discrepancy between in vitro blood calibration data and in vivo blood R_2^* (16). We therefore added a correction factor based on literature values of macroscopic R_2', before conducting the calibration of blood R_2^*. The resulting oxygenation showed good correspondence with the R_2 based TRUST results, suggesting that our assumed macroscopic R_2' is generally valid. However, since shimming condition could vary across brain regions, it would be ideal to conduct macroscopic inhomogeneity correction on a voxel-by-voxel basis (10,46). Since our TRU-PC 3D sequence produced multi-echo data with phase information, we calculated phase maps and further estimated field gradient maps using phase values of adjacent voxels. While these maps provided B_0 inhomogeneity information in the majority of the brain, in regions near and inside veins such computation failed unfortunately. This is because venous voxels have additional susceptibility effects from deoxyhemoglobin, which renders the B_0 inhomogeneity estimation inaccurate. Thus, in order to estimate B_0 inhomogeneity in venous voxels, a higher resolution phase mapping scan, in which each TRU-PC 3D voxel is divided into several sub-voxels, is needed. However, given that our TRU-PC voxel size is already on the order of 1 mm, further dividing it into smaller voxels would be difficult from the standpoint of scan time and image SNR. High resolution used in our TRU-PC 3D sequence does, however, help limit the extent of B_0 inhomogeneity in our data. Furthermore, since we used phase-contrast scheme to isolate sub-voxel venous signal, it is likely that the B_0 inhomogeneity of our venous signal is smaller than that of the entire voxel.

Finally, conversion of blood R_2^* to oxygenation requires the knowledge of hematocrit. Hematocrit would vary across individuals and may alter under certain pathological conditions such as anorexia (38) or Sickle cell anemia (47). Therefore, for accurate estimation of blood oxygenation, it is desirable to measure hematocrit on each individual using either blood sampling or MRI methods (48-50). Furthermore, it is known that microvessels have lower hematocrit values compared to macrovessels (51,52). Because the diameters of the vessels relevant for our study (>1 mm) are much larger than the diameter of a red blood cell (8 μm), we assume that the hematocrit does not change across the vessels that are visible with TRU-PC 3D.

Conclusion

We have developed a quantitative technique to map venous oxygenation in 3D based on blood R_2^* relaxometry. The oxygenation values obtained were consistent with previous reports and also compatible with a validated global method performed on the same participants. Intra-session test-retest assessment revealed good reproducibility of the method. Sensitivity of the method to detect oxygenation alterations due to hyperoxia was demonstrated. This technique may have the potential to monitor oxygenation abnormalities in focal brain diseases.

Supplementary Material

Refer to Web version on PubMed Central for supplementary material.

Acknowledgments

We thank Drs. Susumu Mori and Zhipeng Hou for providing the AMIRA software. We also thank Dr. Hao Huang and Mr. Austin Ouyang for providing the surf format to vtk format conversion script.

Grant Sponsors: NIH R01 MH084021, NIH R01 NS067015, NIH R01 AG042753, NIH R01 AG047972, NIH R21 NS095342, NIH R21 NS085634, and NIH P41 EB015909.

References

1. Derdeyn CP, Videen TO, Grubb RL Jr, Powers WJ. Comparison of PET oxygen extraction fraction methods for the prediction of stroke risk. J Nucl Med. 2001; 42:1195–1197. [PubMed: 11483680]
2. Gupta A, Baradaran H, Schweitzer AD, et al. Oxygen extraction fraction and stroke risk in patients with carotid stenosis or occlusion: a systematic review and meta-analysis. AJNR Am J Neuroradiol. 2014; 35:250–255. [PubMed: 23945227]
3. Leenders KL. PET: blood flow and oxygen consumption in brain tumors. J Neurooncol. 1994; 22:269–273. [PubMed: 7760106]
4. Ishii K, Kitagaki H, Kono M, Mori E. Decreased medial temporal oxygen metabolism in Alzheimer's disease shown by PET. J Nucl Med. 1996; 37:1159–1165. [PubMed: 8965188]
5. Nagata K, Kondoh Y, Atchison R, Sato M, Satoh Y, Watahiki Y, Hirata Y, Yokoyama E. Vascular and metabolic reserve in Alzheimer's disease. Neurobiol Aging. 2000; 21:301–307. [PubMed: 10867215]
6. Thomas BP, Sheng M, Tseng BY, et al. Reduced global brain metabolism but maintained vascular function in amnestic mild cognitive impairment. J Cereb Blood Flow Metab. 2016
7. Mintun MA, Raichle ME, Martin WR, Herscovitch P. Brain oxygen utilization measured with O-15 radiotracers and positron emission tomography. J Nucl Med. 1984; 25:177–187. [PubMed: 6610032]
8. Lu H, Ge Y. Quantitative evaluation of oxygenation in venous vessels using T2-Relaxation-Under-Spin-Tagging MRI. Magn Reson Med. 2008; 60:357–363. [PubMed: 18666116]
9. Fernandez-Seara MA, Techawiboonwong A, Detre JA, Wehrli FW. MR susceptometry for measuring global brain oxygen extraction. Magn Reson Med. 2006; 55:967–973. [PubMed: 16598726]
10. He X, Yablonskiy DA. Quantitative BOLD: mapping of human cerebral deoxygenated blood volume and oxygen extraction fraction: default state. Magn Reson Med. 2007; 57:115–126. [PubMed: 17191227]
11. Gauthier CJ, Hoge RD. Magnetic resonance imaging of resting OEF and CMRO(2) using a generalized calibration model for hypercapnia and hyperoxia. Neuroimage. 2012; 60:1212–1225. [PubMed: 22227047]

12. Wise RG, Harris AD, Stone AJ, Murphy K. Measurement of OEF and absolute CMRO2: MRI-based methods using interleaved and combined hypercapnia and hyperoxia. Neuroimage. 2013; 83:135–147. [PubMed: 23769703]
13. Fan AP, Bilgic B, Gagnon L, Witzel T, Bhat H, Rosen BR, Adalsteinsson E. Quantitative oxygenation venography from MRI phase. Magn Reson Med. 2014; 72:149–159. [PubMed: 24006229]
14. Xu B, Liu T, Spincemaille P, Prince M, Wang Y. Flow compensated quantitative susceptibility mapping for venous oxygenation imaging. Magn Reson Med. 2014; 72:438–445. [PubMed: 24006187]
15. Lu H, Xu F, Grgac K, Liu P, Qin Q, van Zijl P. Calibration and validation of TRUST MRI for the estimation of cerebral blood oxygenation. Magn Reson Med. 2012; 67:42–49. [PubMed: 21590721]
16. Zhao JM, Clingman CS, Narvainen MJ, Kauppinen RA, van Zijl PC. Oxygenation and hematocrit dependence of transverse relaxation rates of blood at 3T. Magn Reson Med. 2007; 58:592–597. [PubMed: 17763354]
17. Chen JJ, Pike GB. Human whole blood T2 relaxometry at 3 Tesla. Magn Reson Med. 2009; 61:249–254. [PubMed: 19165880]
18. Bolar DS, Rosen BR, Sorensen AG, Adalsteinsson E. QUantitative Imaging of eXtraction of oxygen and TIssue consumption (QUIXOTIC) using venular-targeted velocity-selective spin labeling. Magn Reson Med. 2011; 66:1550–1562. [PubMed: 21674615]
19. Krishnamurthy LC, Liu P, Ge Y, Lu H. Vessel-specific quantification of blood oxygenation with T2-relaxation-under-phase-contrast MRI. Magn Reson Med. 2014; 71:978–989. [PubMed: 23568830]
20. Guo J, Wong EC. Venous oxygenation mapping using velocity-selective excitation and arterial nulling. Magn Reson Med. 2012; 68:1458–1471. [PubMed: 22294414]
21. Liu P, Dimitrov I, Andrews T, et al. Multisite evaluations of a T2 -relaxation-under-spin-tagging (TRUST) MRI technique to measure brain oxygenation. Magn Reson Med. 2016; 75:680–687. [PubMed: 25845468]
22. Frank LR, Crawley AP, Buxton RB. Elimination of oblique flow artifacts in magnetic resonance imaging. Magn Reson Med. 1992; 25:299–307. [PubMed: 1614313]
23. Lu W, Yu H, Shimakawa A, Alley M, Reeder SB, Hargreaves BA. Water-fat separation with bipolar multiecho sequences. Magn Reson Med. 2008; 60:198–209. [PubMed: 18581362]
24. Liu H, Lu P, Yezhuvath U, Cheng Y, Marshall O, Ge Y. MRI mapping of cerebrovascular reactivity via gas inhalation challenges. J Vis Exp. 2014
25. Krishnamurthy LC, Mao D, King KS, Lu H. Correction and optimization of a T2-based approach to map blood oxygenation in small cerebral veins. Magn Reson Med. 2016; 75:1100–1109. [PubMed: 25846113]
26. Ayachit, U. The ParaView Guide: A Parallel Visualization Application. Kitware, Inc; 2015. p. 276
27. Benga G, Borza T. Diffusional water permeability of mammalian red blood cells. Comp Biochem Physiol B Biochem Mol Biol. 1995; 112:653–659. [PubMed: 8590380]
28. Krishnamurthy LC, Liu P, Xu F, Uh J, Dimitrov I, Lu H. Dependence of blood T(2) on oxygenation at 7 T: in vitro calibration and in vivo application. Magn Reson Med. 2014; 71:2035–2042. [PubMed: 23843129]
29. Silvennoinen MJ, Clingman CS, Golay X, Kauppinen RA, van Zijl PC. Comparison of the dependence of blood R2 and R2* on oxygen saturation at 1.5 and 4.7 Tesla. Magn Reson Med. 2003; 49:47–60. [PubMed: 12509819]
30. Wansapura JP, Holland SK, Dunn RS, Ball WS Jr. NMR relaxation times in the human brain at 3.0 tesla. J Magn Reson Imaging. 1999; 9:531–538. [PubMed: 10232510]
31. Lu H, Xu F, Rodrigue KM, Kennedy KM, Cheng Y, Flicker B, Hebrank AC, Uh J, Park DC. Alterations in cerebral metabolic rate and blood supply across the adult lifespan. Cereb Cortex. 2011; 21:1426–1434. [PubMed: 21051551]
32. Gibbs EL, Lennox WG, Nims LF, Gibbs FA. Arterial and cerebral venous blood - Arterial-venous differences in man. J Biol Chem. 1942; 144:325–332.

33. Ibaraki M, Miura S, Shimosegawa E, Sugawara S, Mizuta T, Ishikawa A, Amano M. Quantification of cerebral blood flow and oxygen metabolism with 3-dimensional PET and 15O: validation by comparison with 2-dimensional PET. J Nucl Med. 2008; 49:50–59. [PubMed: 18077532]
34. Albers, R., Siegel, G. Basic Neurochemistry: Molecular, cellular and medical aspects. Philadelphia, PA: Lippincott Williams & Wilkins; 1999.
35. Ge Y, Zhang Z, Lu H, Tang L, Jaggi H, Herbert J, Babb JS, Rusinek H, Grossman RI. Characterizing brain oxygen metabolism in patients with multiple sclerosis with T2-relaxation-under-spin-tagging MRI. J Cereb Blood Flow Metab. 2012; 32:403–412. [PubMed: 22252237]
36. Pascual JM, Liu P, Mao D, et al. Triheptanoin for glucose transporter type I deficiency (G1D): modulation of human ictogenesis, cerebral metabolic rate, and cognitive indices by a food supplement. JAMA Neurol. 2014; 71:1255–1265. [PubMed: 25110966]
37. Bush AM, Borzage M, Choi S, Coates T, Wood JC. Elevated Cerebral Metabolic Oxygen Consumption in Sickle Cell Disease. Blood. 2014; 124:2706–2706.
38. Sheng M, Lu H, Liu P, Thomas BP, McAdams CJ. Cerebral perfusion differences in women currently with and recovered from anorexia nervosa. Psychiatry Res. 2015; 232:175–183. [PubMed: 25795596]
39. Zheng G, Wen J, Lu H, et al. Elevated global cerebral blood flow, oxygen extraction fraction and unchanged metabolic rate of oxygen in young adults with end-stage renal disease: an MRI study. Eur Radiol. 2016; 26:1732–1741. [PubMed: 26334507]
40. Jain V, Buckley EM, Licht DJ, et al. Cerebral oxygen metabolism in neonates with congenital heart disease quantified by MRI and optics. J Cereb Blood Flow Metab. 2014; 34:380–388. [PubMed: 24326385]
41. Liu P, Lu H, Filbey FM, Tamminga CA, Cao Y, Adinoff B. MRI assessment of cerebral oxygen metabolism in cocaine-addicted individuals: hypoactivity and dose dependence. NMR Biomed. 2014; 27:726–732. [PubMed: 24757009]
42. Gideon P, Thomsen C, Gjerris F, Sorensen PS, Stahlberg F, Henriksen O. Measurement of blood flow in the superior sagittal sinus in healthy volunteers, and in patients with normal pressure hydrocephalus and idiopathic intracranial hypertension with phase-contrast cine MR imaging. Acta Radiol. 1996; 37:171–176. [PubMed: 8600956]
43. Stolz E, Kaps M, Kern A, Babacan SS, Dorndorf W. Transcranial color-coded duplex sonography of intracranial veins and sinuses in adults. Reference data from 130 volunteers Stroke. 1999; 30:1070–1075. [PubMed: 10229746]
44. Yamada K, Naruse S, Nakajima K, Furuya S, Morishita H, Kizu O, Maeda T, Takeo K, Shimizu K. Flow velocity of the cortical vein and its effect on functional brain MRI at 1.5T: preliminary results by cine-MR venography. J Magn Reson Imaging. 1997; 7:347–352. [PubMed: 9090589]
45. Haacke, EM., Brown, RW., Thompson, MR., Venkatesan, R. Magnetic resonance imaging : physical principles and sequence design. New York: Wiley; 1999. p. 931-932.
46. Yablonskiy DA, Sukstanskii AL, Luo J, Wang X. Voxel spread function method for correction of magnetic field inhomogeneity effects in quantitative gradient-echo-based MRI. Magn Reson Med. 2013; 70:1283–1292. [PubMed: 23233445]
47. Jordan LC, Gindville MC, Scott AO, et al. Non-invasive imaging of oxygen extraction fraction in adults with sickle cell anaemia. Brain. 2016; 139:738–750. [PubMed: 26823369]
48. Qin Q, Grgac K, van Zijl PC. Determination of whole-brain oxygen extraction fractions by fast measurement of blood T(2) in the jugular vein. Magn Reson Med. 2011; 65:471–479. [PubMed: 21264936]
49. Wu WC, Jain V, Li C, Giannetta M, Hurt H, Wehrli FW, Wang DJ. In vivo venous blood T1 measurement using inversion recovery true-FISP in children and adults. Magn Reson Med. 2010; 64:1140–1147. [PubMed: 20564586]
50. Varela M, Hajnal JV, Petersen ET, Golay X, Merchant N, Larkman DJ. A method for rapid in vivo measurement of blood T1. NMR Biomed. 2011; 24:80–88. [PubMed: 20669148]
51. Oldendorf WH, Kitano M, Shimizu S, Oldendorf SZ. Hematocrit of the human cranial blood pool. Circ Res. 1965; 17:532–539. [PubMed: 5843886]
52. Sarelius IH, Duling BR. Direct measurement of microvessel hematocrit, red cell flux, velocity, and transit time. Am J Physiol. 1982; 243:H1018–1026. [PubMed: 7149038]

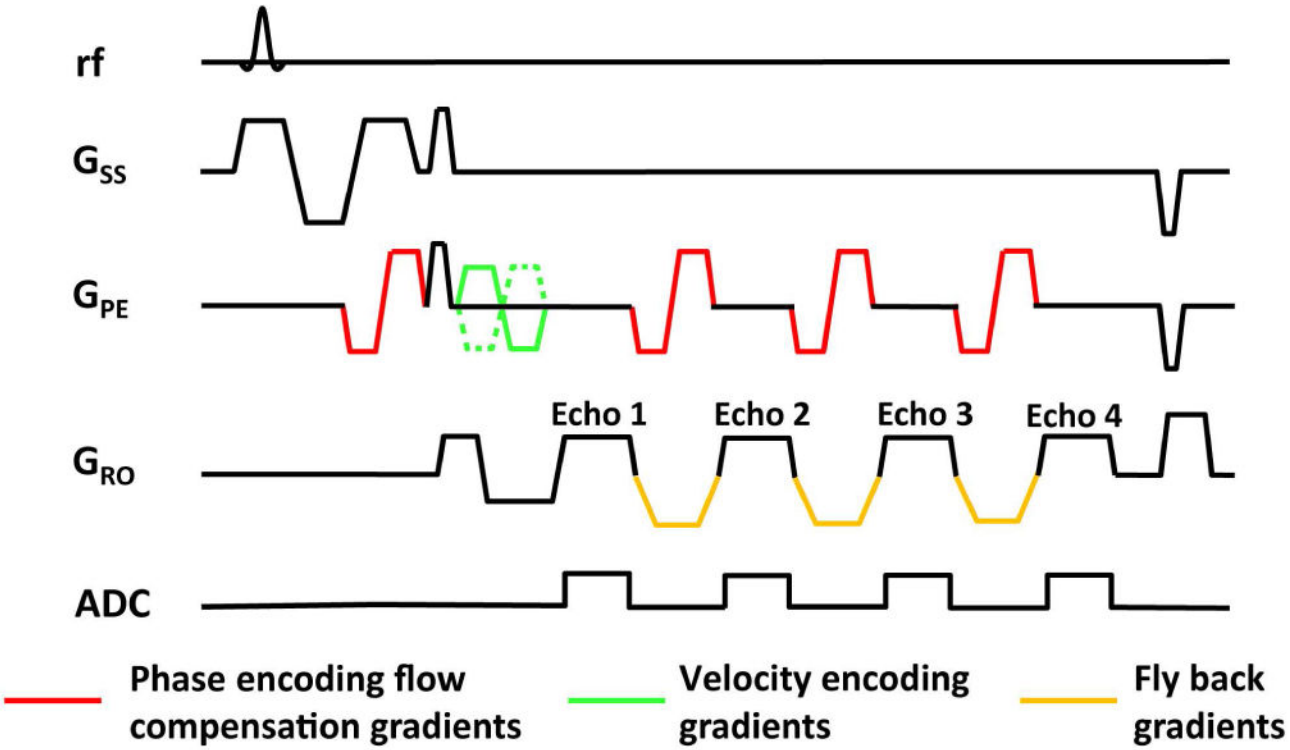

Figure 1.
Sequence diagram of TRU-PC 3D. Key sequence components are displayed in color.

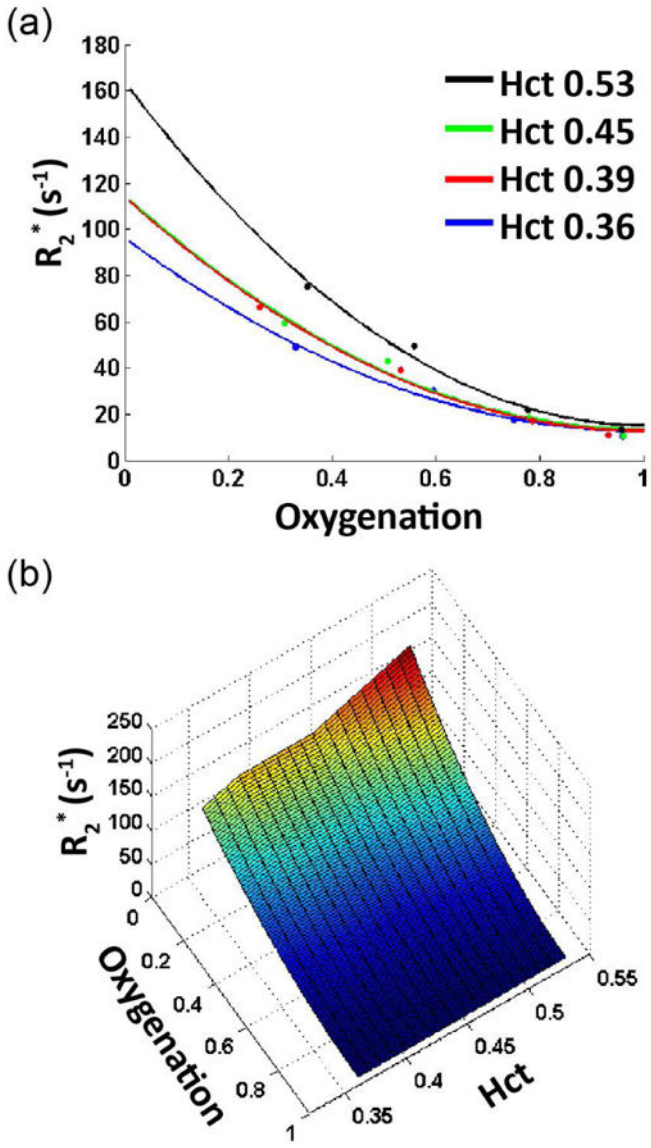

Figure 2.

Summary of in vitro blood experiments. (a) R_2^* as a function of blood oxygen (Y) at several Hct levels. (b) Three-dimensional relationship among R_2^*, Y, and Hct.

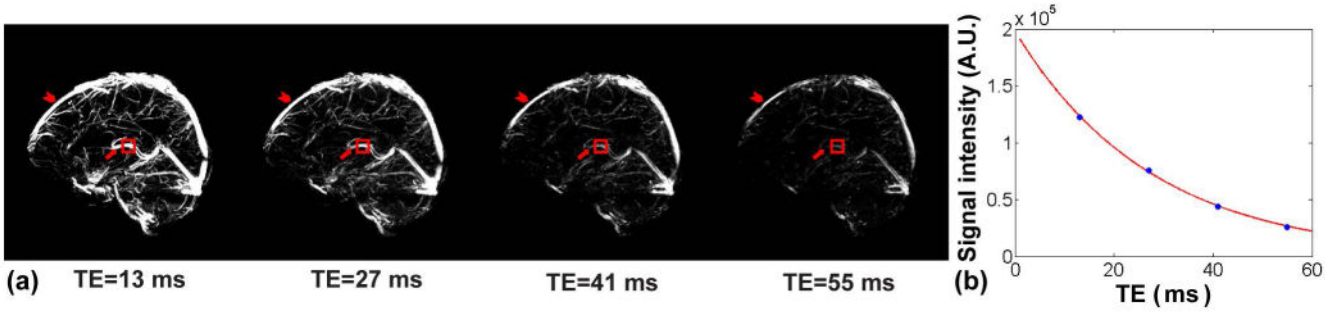

Figure 3.

Representative TRU-PC 3D data in volunteer. (a) Complex difference images from TRU-PC 3D as a function of TE. The complex difference image of the sequence is expected to contain signals from vessel only. Images have been maximum-intensity projected for display purpose. Arrow head indicates superior sagittal sinus. Arrow indicates internal cerebral veins. Red box indicates ROI from which the data of Panel b is derived. (b) Complex difference MR signal as a function of TE. The solid curve indicates the fitting results.

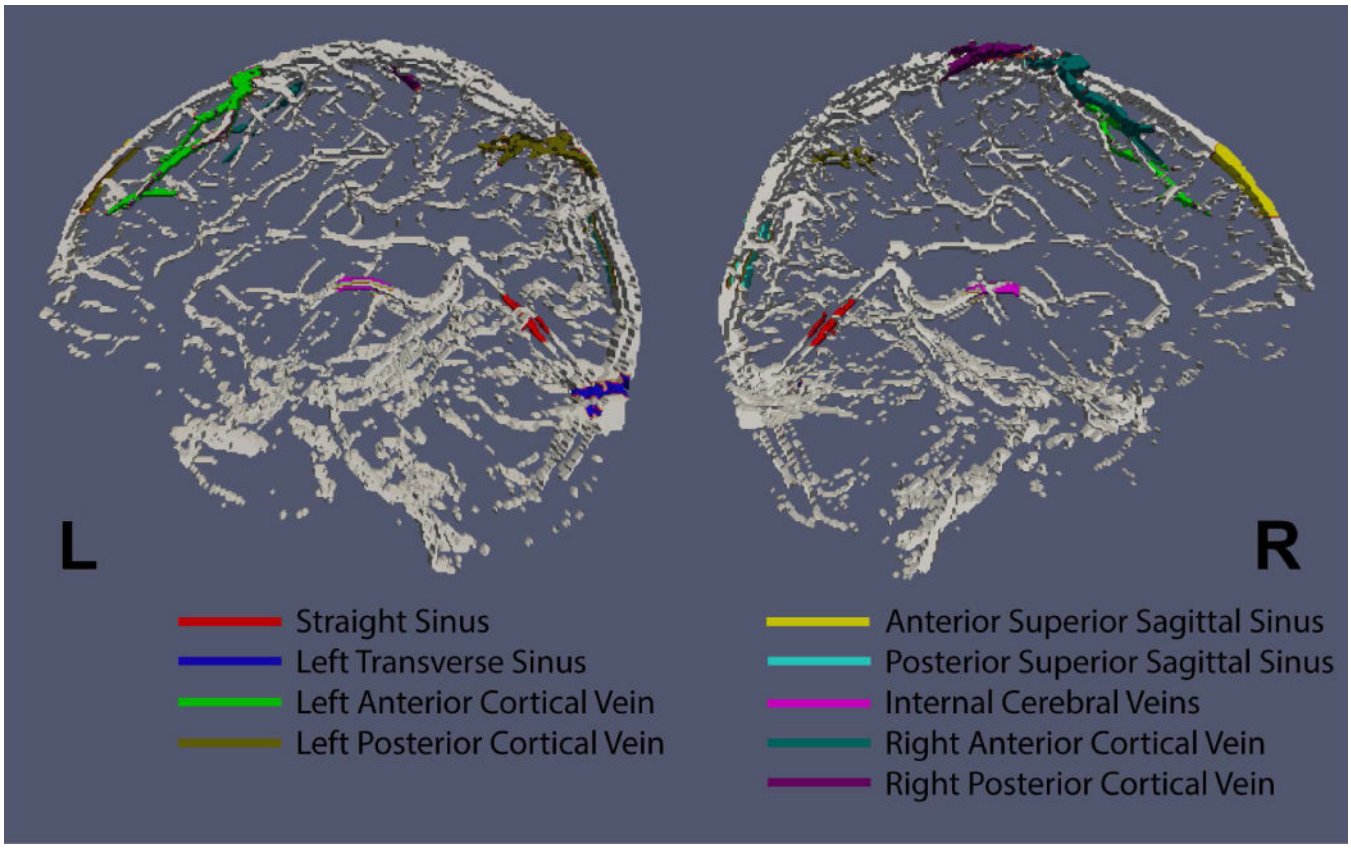

Figure 4.
Regions of interest (in color) overlaid on complex difference image. The ROIs were drawn manually and the signals within each ROI were averaged and fitted. The resulting oxygenation values are listed in Table 2.

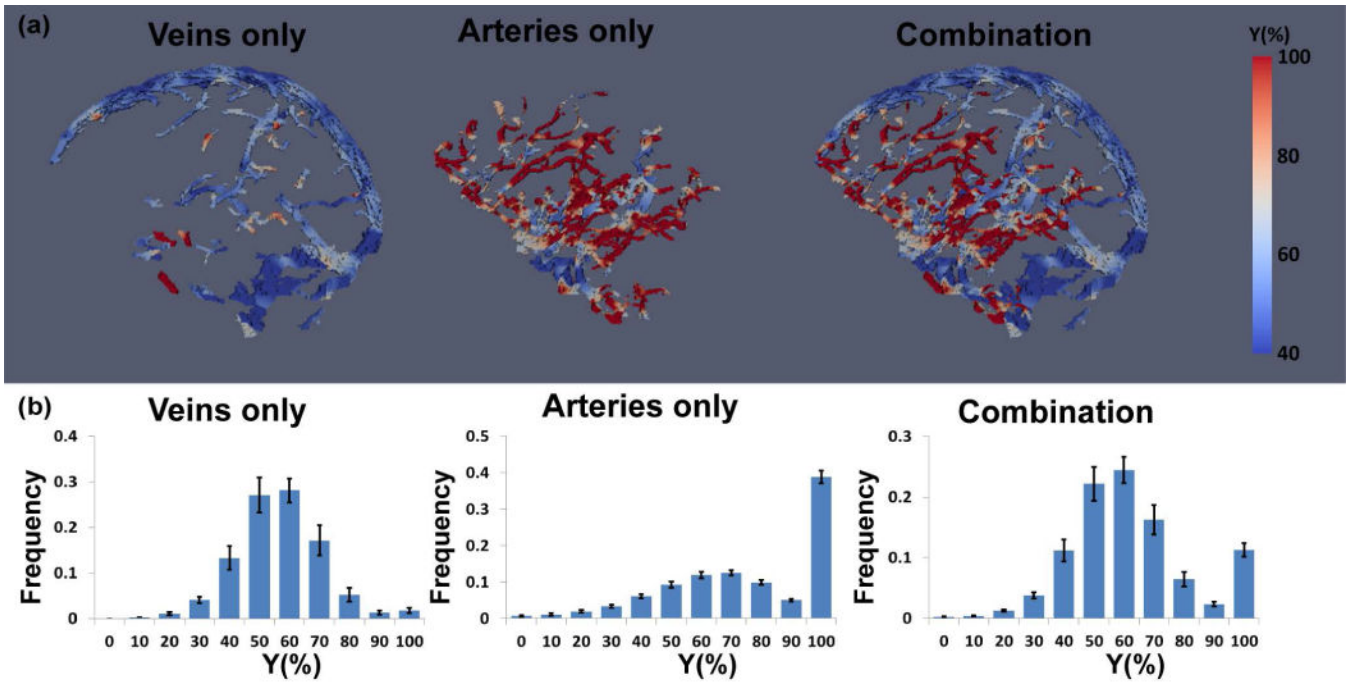

Figure 5.

Quantitative oxygenation maps obtained from TRU-PC 3D. (a) An example of 3D oxygenation maps of veins only, arteries only, and their combination. (b) Histogram of oxygenation values in each map. The results of all participants were averaged, with error bars indicating standard errors across individuals.

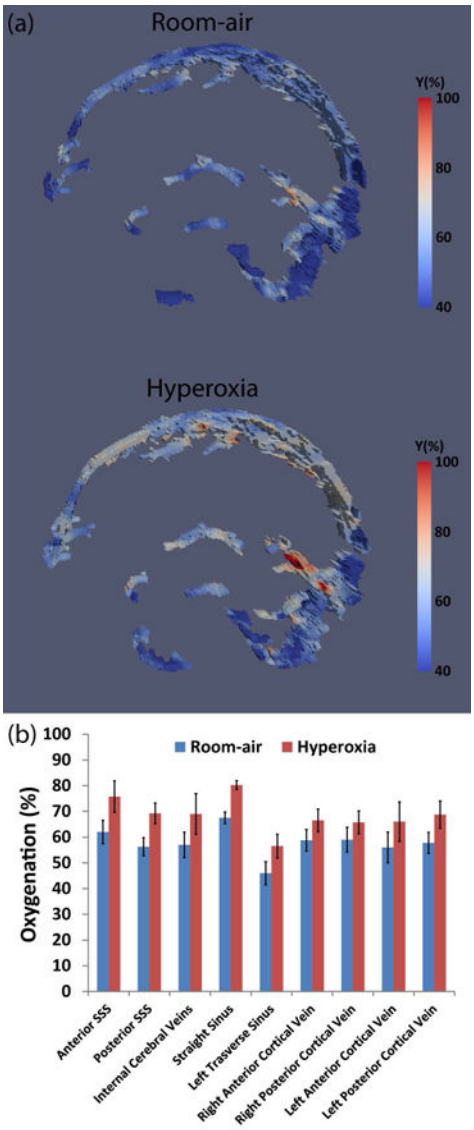

Figure 6.

Summary of TRU-PC 3D results during hyperoxia challenge. (a) Representative venous oxygenation maps under normoxia and hyperoxia. (b) Region of interest results for nine ROIs. Error bars indicate standard errors. SSS: Superior sagittal sinus.

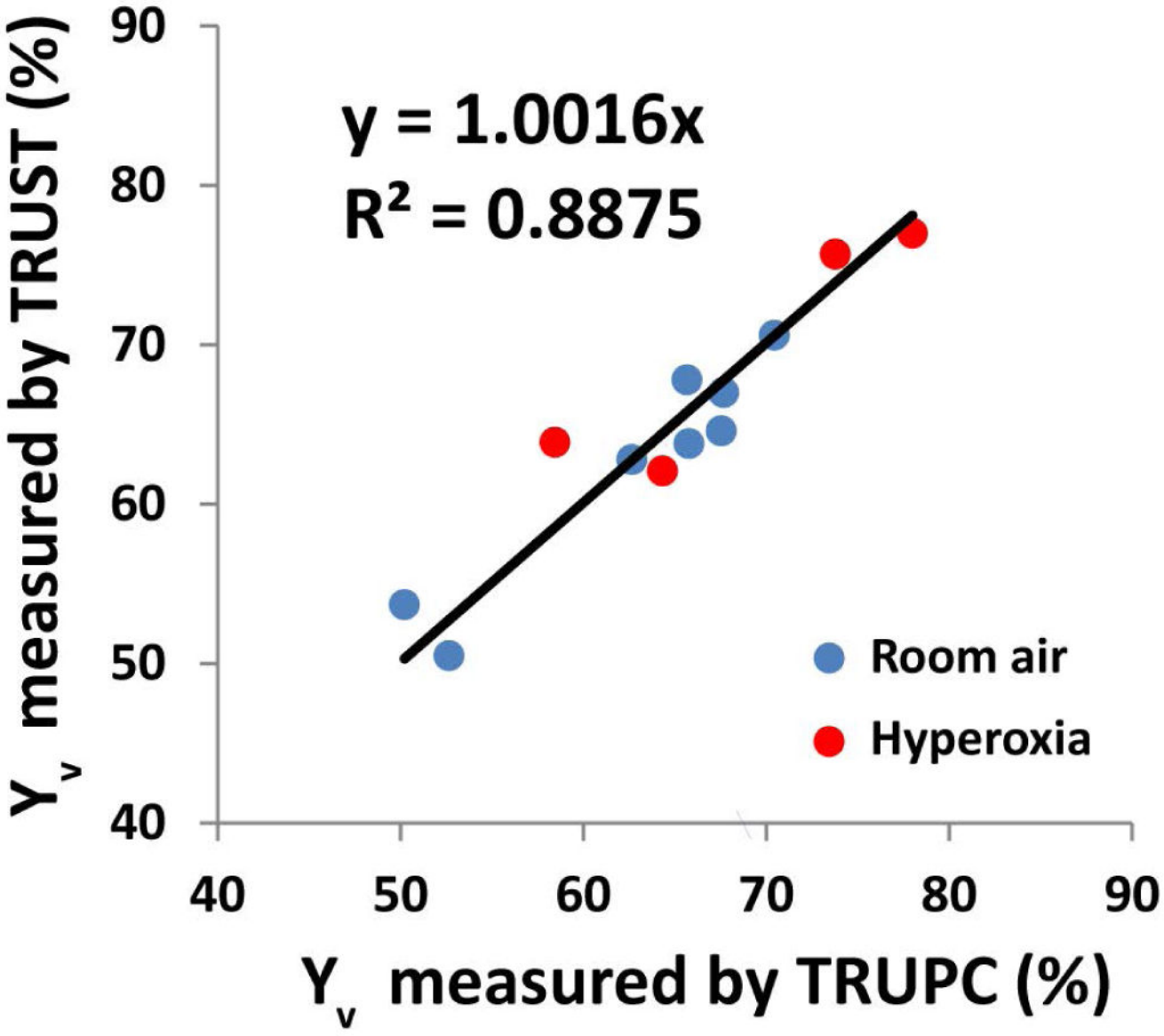

Figure 7.

Scatter plot between oxygenation values measured with TRU-PC 3D and those from TRUST MRI. Blue dots represent results under room-air breathing. Red dots represent results under hyperoxia. Four subjects participated in both room-air and hyperoxia experiments. Four additional subjects participated in room-air only.

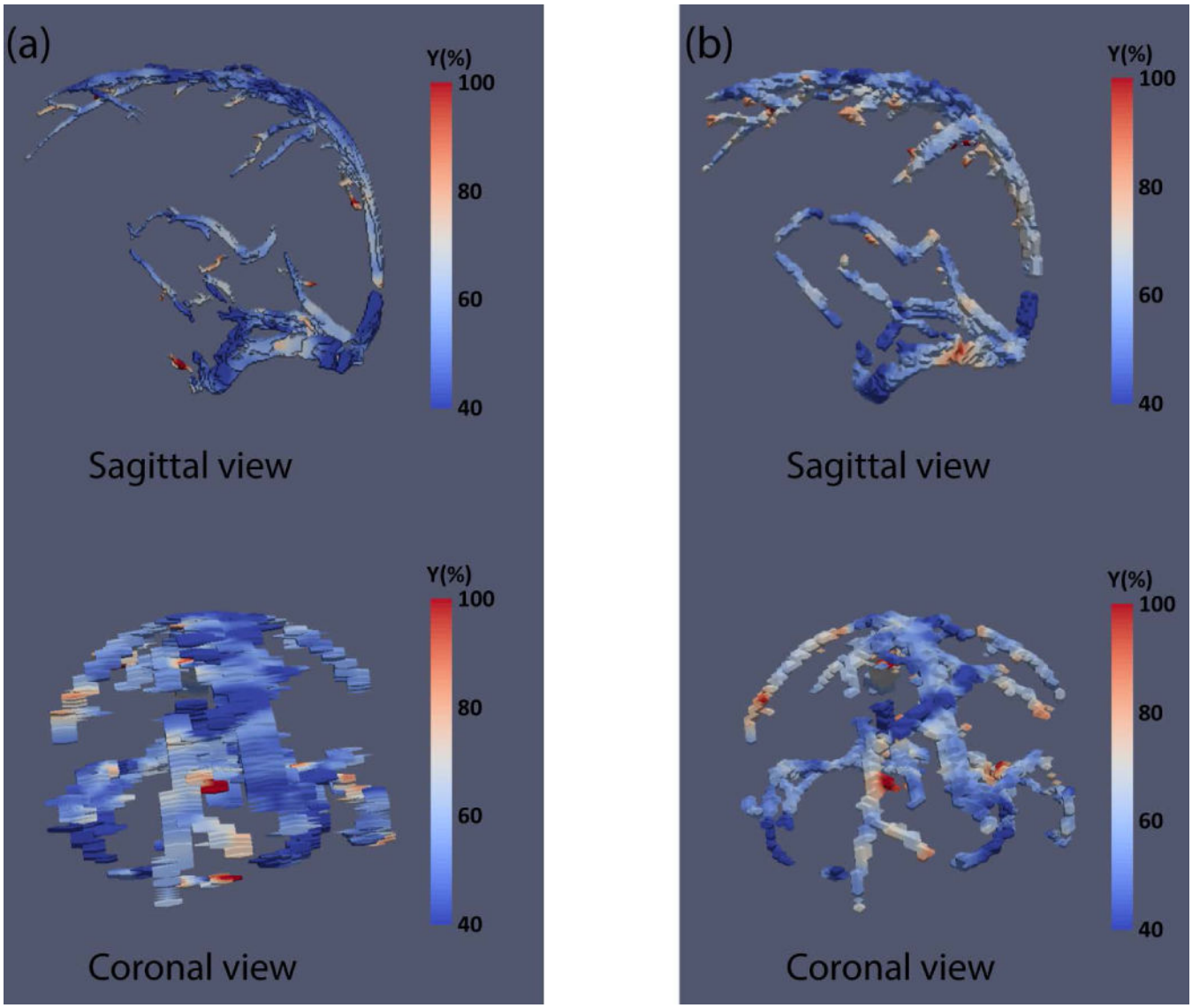

Figure 8.

Y_v maps from one representative subject using two spatial resolutions. (a) voxel size $0.7\times0.7\times5$ mm^3; (b) voxel size $1.5\times1.5\times2$ mm^3. Top panels show sagittal view and bottom panels show coronal view.

Table 1

Fitted coefficients describing the relationship between blood R_2^* and oxygenation for different Hct levels.

Hct level	A (s^{-1})	C (s^{-1})
36%	12.6	83.5
39%	12.7	101.1
45%	13.4	101.2
53%	15.2	148.5

Table 2

Region-of-interest oxygenation values and test-retest reproducibility (in CoV) for 9 venous structures delineated in Figure 4.

ROI Location	Y_v	CoV
Anterior Superior Sagittal Sinus	71.3%±4.9%	2.9%
Posterior Superior Sagittal Sinus	64.8%±11.0%	5.4%
Internal Cerebral Veins	69.3%±8.9%	2.4%
Straight Sinus	72.0%±9.3%	3.5%
Left Transverse Sinus	57.0%±7.9%	2.6%
Right Anterior Cortical Vein	70.25%±3.0%	1.8%
Right Posterior Cortical Vein	68.3%±4.3%	2.3%
Left Anterior Cortical Vein	70.3%±2.2%	3.1%
Left Posterior Cortical Vein	67.8%±7.8%	3.3%